

# Measurement of electron neutrino quasielastic and quasielastic-like scattering on hydrocarbon at $\langle E_\nu \rangle = 3.6$ GeV

J. Wolcott,<sup>1</sup> O. Altinok,<sup>2</sup> L. Bellantoni,<sup>3</sup> A. Bercellie,<sup>1</sup> M. Betancourt,<sup>3</sup> A. Bodek,<sup>1</sup>  
 A. Bravar,<sup>4</sup> H. Budd,<sup>1</sup> M.F. Carneiro,<sup>5</sup> J. Chvojka,<sup>1</sup> H. da Motta,<sup>5</sup> J. Devan,<sup>6</sup>  
 S.A. Dytman,<sup>7</sup> G.A. Díaz,<sup>1,8</sup> B. Eberly,<sup>7,\*</sup> J. Felix,<sup>9</sup> L. Fields,<sup>3,10</sup> R. Fine,<sup>1</sup> R. Galindo,<sup>11</sup>  
 H. Gallagher,<sup>2</sup> A. Ghosh,<sup>5,1</sup> T. Golan,<sup>1,3</sup> R. Gran,<sup>12</sup> D.A. Harris,<sup>3</sup> A. Higuera,<sup>1,9,†</sup>  
 M. Kiveni,<sup>3</sup> J. Kleykamp,<sup>1</sup> M. Kordosky,<sup>6</sup> T. Le,<sup>2,13</sup> E. Maher,<sup>14</sup> S. Manly,<sup>1</sup>  
 W.A. Mann,<sup>2</sup> C.M. Marshall,<sup>1</sup> D.A. Martinez Caicedo,<sup>3,‡</sup> K.S. McFarland,<sup>1,3</sup>  
 C.L. McGivern,<sup>7</sup> A.M. McGowan,<sup>1</sup> B. Messerly,<sup>7</sup> J. Miller,<sup>11</sup> A. Mislivec,<sup>1</sup> J.G. Morfín,<sup>3</sup>  
 J. Mousseau,<sup>15</sup> T. Muhlbeier,<sup>5</sup> D. Naples,<sup>7</sup> J.K. Nelson,<sup>6</sup> A. Norrick,<sup>6</sup> J. Osta,<sup>3</sup>  
 V. Paolone,<sup>7</sup> J. Park,<sup>1</sup> C.E. Patrick,<sup>10</sup> G.N. Perdue,<sup>3,1</sup> L. Rakotondravohitra,<sup>3,§</sup>  
 R.D. Ransome,<sup>13</sup> H. Ray,<sup>15</sup> L. Ren,<sup>7</sup> D. Rimal,<sup>15</sup> P.A. Rodrigues,<sup>1</sup> D. Ruterbories,<sup>1</sup>  
 H. Schellman,<sup>16,10</sup> D.W. Schmitz,<sup>17,3</sup> C.J. Solano Salinas,<sup>18</sup> N. Tagg,<sup>19</sup> B.G. Tice,<sup>13</sup>  
 E. Valencia,<sup>9</sup> T. Walton,<sup>20,¶</sup> M. Wospakrik,<sup>15</sup> G. Zavala,<sup>9</sup> D. Zhang,<sup>6</sup> and B.P. Ziemer<sup>21</sup>

(The MINERvA Collaboration)

<sup>1</sup>*University of Rochester, Rochester, New York 14627 USA*

<sup>2</sup>*Physics Department, Tufts University, Medford, Massachusetts 02155, USA*

<sup>3</sup>*Fermi National Accelerator Laboratory, Batavia, Illinois 60510, USA*

<sup>4</sup>*University of Geneva, 1211 Geneva 4, Switzerland*

<sup>5</sup>*Centro Brasileiro de Pesquisas Físicas, Rua Dr. Xavier Sigaud  
150, Urca, Rio de Janeiro, Rio de Janeiro, 22290-180, Brazil*

<sup>6</sup>*Department of Physics, College of William & Mary, Williamsburg, Virginia 23187, USA*

<sup>7</sup>*Department of Physics and Astronomy, University  
of Pittsburgh, Pittsburgh, Pennsylvania 15260, USA*

<sup>8</sup>*Sección Física, Departamento de Ciencias, Pontificia  
Universidad Católica del Perú, Apartado 1761, Lima, Perú*

<sup>9</sup>*Campus León y Campus Guanajuato, Universidad de Guanajuato, Lascurain  
de Retana No. 5, Colonia Centro, Guanajuato 36000, Guanajuato México.*

<sup>10</sup>*Northwestern University, Evanston, Illinois 60208*

<sup>11</sup>*Departamento de Física, Universidad Técnica Federico Santa  
María, Avenida España 1680 Casilla 110-V, Valparaíso, Chile*

<sup>12</sup>*Department of Physics, University of Minnesota – Duluth, Duluth, Minnesota 55812, USA*

<sup>13</sup>*Rutgers, The State University of New Jersey, Piscataway, New Jersey 08854, USA*

<sup>14</sup>*Massachusetts College of Liberal Arts, 375 Church Street, North Adams, MA 01247*

<sup>15</sup>*University of Florida, Department of Physics, Gainesville, FL 32611*

<sup>16</sup>*Department of Physics, Oregon State University, Corvallis, Oregon 97331, USA*

<sup>17</sup>*Enrico Fermi Institute, University of Chicago, Chicago, IL 60637 USA*

<sup>18</sup>*Universidad Nacional de Ingeniería, Apartado 31139, Lima, Perú*

<sup>19</sup>*Department of Physics, Otterbein University, 1  
South Grove Street, Westerville, OH, 43081 USA*

<sup>20</sup>*Hampton University, Dept. of Physics, Hampton, VA 23668, USA*

<sup>21</sup>*Department of Physics and Astronomy, University of  
California, Irvine, Irvine, California 92697-4575, USA*

(Dated: December 8, 2024)

## Abstract

The first direct measurement of electron-neutrino quasielastic and quasielastic-like scattering on hydrocarbon in the few-GeV region of incident neutrino energy has been carried out using the MINERvA detector in the NuMI beam at Fermilab. The flux-integrated differential cross sections in electron production angle, electron energy and  $Q^2$  are presented. The ratio of the quasielastic, flux-integrated differential cross section in  $Q^2$  for  $\nu_e$  with that of similarly-selected  $\nu_\mu$ -induced events from the same exposure is used to probe assumptions that underpin conventional treatments of charged-current  $\nu_e$  interactions used by long-baseline neutrino oscillation experiments. The data are found to be consistent with lepton universality and are well-described by the predictions of the neutrino event generator GENIE.

**PACS numbers:** 13.15.+g,25.30.Pt

---

\* now at SLAC National Accelerator Laboratory, Stanford, California 94309 USA

† University of Houston, Houston, Texas, 77204, USA

‡ Now at Illinois Institute of Technology

§ also at Department of Physics, University of Antananarivo, Madagascar

¶ now at Fermi National Accelerator Laboratory, Batavia, IL USA 60510

## I. INTRODUCTION

Current and future neutrino oscillation experiments hope to measure CP violation in the neutrino sector by making precise measurements of  $\nu_e(\bar{\nu}_e)$  appearance in predominantly  $\nu_\mu(\bar{\nu}_\mu)$  beams. These experiments (such as NOvA[1], T2K[2], and DUNE[3]) consist of large detectors of heavy nuclei (e.g., carbon, oxygen, argon) to maximize the rate of neutrino interactions. They examine the energy distribution of interacting neutrinos and compare the observed spectrum with the predictions based on different oscillation hypotheses. Correct prediction of the observed energy spectrum for  $\nu_e$  interactions requires an accurate model of the interaction rates, particle content, multiplicity and outgoing particle kinematics. In other words, there is a need for precise  $\nu_e$  cross sections on the appropriate detector materials.

The relatively small components of  $\nu_e$  and  $\bar{\nu}_e$  flux in neutrino beams coupled with significant backgrounds arising from the dominant  $\nu_\mu$  interactions have led to a paucity of  $\nu_e$  and  $\bar{\nu}_e$  measurements in this energy range (0.5 to a few GeV). Gargamelle[4] and T2K[5] have published  $\nu_e$  inclusive cross-section measurements at these energies, but small statistics and the inclusive nature of both of these measurements limit their usefulness for model comparisons and as a basis for tuning simulations. Therefore, most simulations, such as those used in oscillation experiments, begin by tuning to high-precision  $\nu_\mu(\bar{\nu}_\mu)$  cross section data and apply corrections such as those discussed in Ref. [6] to obtain a prediction for the  $\nu_e(\bar{\nu}_e)$  cross section.

This paper reports measurements of  $\nu_e$  and  $\bar{\nu}_e$  charged-current quasielastic (CCQE) interactions ( $\nu_e n \rightarrow e^- p$  and  $\bar{\nu}_e p \rightarrow e^+ n$ ) on nucleons in a hydrocarbon target at an average  $\nu_e$  energy of 3.6 GeV. Quasielastic scattering is a two-body process that is of particular importance in neutrino physics. Though the incoming neutrino has an unknown energy and the final state nucleon may not be detected, knowledge of the incoming neutrino direction and the outgoing lepton momentum vector, along with the assumption that the initial state nucleon is at rest, are sufficient to constrain the kinematics. The quasielastic process is the dominant reaction near 1 GeV, which is a critical energy region for accelerator-based long-baseline oscillation experiments. The assumption that quasielastic scattering takes place on free, stationary nucleons is often used to extract an accurate estimate of the neutrino energy ( $E_\nu^{\text{QE}}$ ). However, hadrons exiting the nucleus after the interaction can reinteract and change identity or eject other hadrons[7], and pairs of nucleons correlated within the

initial state may cause multiple nucleons to be ejected by a single interaction[8, 9]. Thus, true quasielastic events cannot be reliably isolated experimentally. As an alternative, this analysis defines “CCQE-like” events to be the signal. These are events having a prompt electron or positron from the primary vertex plus any number of nucleons, but devoid of any other hadrons or associated gamma conversions. Both  $\nu_e$  and  $\bar{\nu}_e$ -induced CCQE-like events are included since the final-state  $e^\pm$  cannot be distinguished in MINERvA’s unmagnetized tracking volume. The  $\bar{\nu}_e$  have a significantly smaller flux and cross section relative to the  $\nu_e$ , though there is a small analysis selection bias favoring  $\bar{\nu}_e$  over  $\nu_e$ . According to simulation the  $\bar{\nu}_e$ -induced events comprise 8.9% of the selected sample of  $\nu_e$  and  $\bar{\nu}_e$  interactions. In this paper, the  $\bar{\nu}_e$  (positron) content is included when referring to the signal.

The relatively high statistics in the MINERvA data set allows for flux-integrated differential cross section measurements for the  $\nu_e$  quasielastic-like process as well as a comparison of the  $\nu_e$  and  $\nu_\mu$  quasielastic cross sections as a function of  $Q^2$ . These measurements are useful for neutrino oscillation experiments seeking to quantify their understanding of the expected  $\nu_e$  energy distribution. Notably, the target medium for this analysis (hydrocarbon) is nearly identical to that used in NOvA and the T2K near detector, and the neutrino energy range of this analysis overlaps that of NOvA and DUNE.

## II. THE MINERVA EXPERIMENT

MINERvA records interactions of neutrinos produced in the NuMI beam line[10]. In NuMI, a beam of 120-GeV protons strikes a graphite target and produces charged mesons which are focused by two magnetic horns into a 675-m helium-filled decay pipe where most of the charged mesons decay producing neutrinos. For the data used in this analysis, the horns focused positive mesons, resulting in a beam enriched in neutrinos with a most probable neutrino energy of 3.1 GeV. This analysis uses data taken between March 2010 and April 2012 with  $3.49 \times 10^{20}$  POT (protons on target).

The neutrino beam is simulated by a GEANT4-based model[11, 12] constrained to reproduce hadron production measurements[13–21]. Hadronic interactions not constrained by the external hadron production measurements are predicted using the FTFP hadron shower model[22]. The uncertainty on the prediction of the neutrino flux depends upon the precision in these hadron production measurements, uncertainties in the beam line focusing system

and alignment[23], and comparisons between different hadron production models in regions not covered by the external data. Recently, an *in situ* MINERvA measurement of purely leptonic  $\nu - e$  elastic scattering from atomic electrons[24] became available and is used to provide a data-based constraint for the flux estimate. The calculated  $\nu_e + \bar{\nu}_e$  flux for this analysis is shown in Fig. 1.

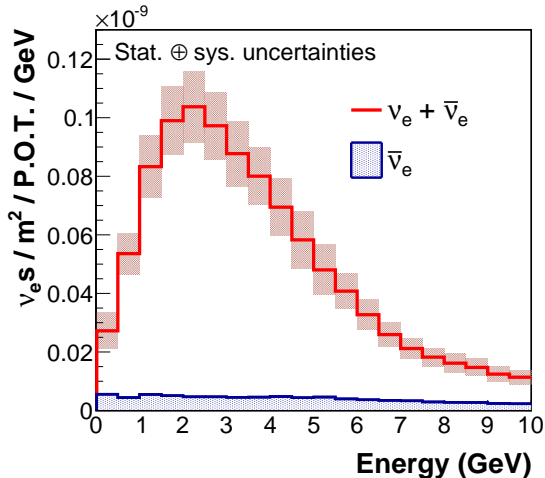


FIG. 1. The  $\nu_e + \bar{\nu}_e$  flux as a function of neutrino energy from the beam simulation for the data used in this analysis. The  $\bar{\nu}_e$  flux is shown separately to emphasize the dominance of  $\nu_e$  in the sum.

The MINERvA detector consists of a core of scintillator strips surrounded by electromagnetic and hadronic calorimeters on the sides and downstream end of the detector. The target and tracking region for this analysis is 95% CH and 5% other materials by weight. The triangular  $3.4 \times 1.7 \text{ cm}^2$  strips are approximately perpendicular to the beam axis and are arranged in hexagonal planes of three orientations, enabling stereoscopic reconstruction of the neutrino interaction vertex and outgoing charged tracks. The downstream electromagnetic calorimeter (ECAL) is identical to the tracking region except for the addition of a 0.2-cm (0.35 radiation lengths) lead sheet in front of every two planes of scintillator.

MINERvA is located 2 m upstream of the MINOS near detector, a magnetized iron spectrometer[25], which is used to reconstruct the momentum and charge of  $\mu^\pm$ . The MINERvA detector's response is simulated by a tuned GEANT4-based[11, 12] program. The energy scale of the detector is set by ensuring that both the photostatistics and the reconstructed energy deposited by momentum-analyzed beam-related muons traversing the

detector agree in data and simulation. The calorimetric constants used to reconstruct the energy of electromagnetic showers, including corrections for passive material[26] and algorithm-specific tuning, are determined from the simulation. Detailed descriptions of the MINERvA detector configuration, calibrations and performance can be found in [26–28].

Neutrino interactions are simulated using the GENIE 2.6.2 event generator[29]. The simulation is used for efficiency corrections, unfolding, and background estimation. Weak interaction (V-A) phenomenology is used for quasielastic interactions[30] in the simulation, with axial mass  $M_A=0.99$  GeV and a relativistic Fermi gas nuclear model. The modeled charged-current cross sections differ for  $\nu_e$  and  $\nu_\mu$  only in the lepton mass, which appears in kinematic factors in the differential cross section expressions.

### III. EVENT RECONSTRUCTION AND ANALYSIS

Events selected for this analysis are required to originate from a 5.57-ton fiducial volume in the central scintillator region of MINERvA. The energy depositions in the scintillator strips (hits) are first grouped in time and then spatially grouped into clusters of energy in each scintillator plane. Clusters with energy  $> 1$  MeV are matched among the three views to create tracks. The hits in each scintillator strip are recorded with 3.0-ns timing resolution, allowing separation of multiple interactions within a single beam spill. Candidate events are created from tracks whose most upstream energy deposition is in the fiducial volume and which do not exit the back of the detector, as such highly penetrating tracks are overwhelmingly muons. All tracks passing the criteria above are tested as  $e^\pm$  candidates. Hits within a  $7.5^\circ$  cone (of minimum radius 50 mm) with an apex at the event vertex and a symmetry axis along the track direction are considered. Hits are associated with the cone as it extends through the scintillator tracker and ECAL; the collection of hits ceases when a gap of three radiation lengths is encountered that is devoid of hits. The hits in this cone ‘object’ are examined using a multivariate particle identification (PID) algorithm. This technique combines details of the energy deposition pattern both longitudinally (mean  $dE/dx$  and the fraction of energy at the downstream end of cone) and transverse to the axis of the cone (mean shower width) using a  $k$ -nearest-neighbors (kNN) algorithm[31]. For those candidate events deemed consistent with an electromagnetic cascade, electrons and positrons are separated from photons by demanding the energy deposition near the upstream end of

the cone be consistent with a single track rather than the two particles expected from photon conversion to  $e^+e^-$ . The discriminant used for this separation is the minimum energy in a sliding 100-mm window along the axis of the cone, in 20 mm steps, from the event origin up to 500 mm (about 1.2 radiation lengths). This technique reduces the possibility of bias introduced by nuclear activity near the interaction point[32]. Cone objects surviving to this point are considered to be electron (or positron) candidates.

The next stage of the analysis requires the topology of the event to be consistent with  $\nu_e$  CCQE-like. Events containing tracks consistent with charged pions or muons, or events with electromagnetic activity outside of the electron candidate cone object (such as might be expected in the presence of a  $\pi^0$  decay) are removed by a cut on the “extra energy ratio” variable  $\Psi$ . This quantity represents the relative amount of energy outside the electron candidate cone to that inside the electron candidate cone. Hits within a sphere of 30-cm radius about the interaction vertex are ignored when calculating  $\Psi$  to reduce the contribution from low-energy nucleons which are potentially not well simulated [32]. Events at large  $\Psi$  are removed from the sample. The cut in  $\Psi$  is a function of the total visible energy of the event and was tuned using simulated events. In addition to the  $\Psi$  cut, Michel electron candidates from the  $\pi \rightarrow \mu \rightarrow e$  decay chain are rejected via timing and their spatial proximity to track ends.

Finally, events are retained in the sample only if they have a reconstructed electron energy  $E_e$  greater than 0.5 GeV and a reconstructed neutrino energy  $E_\nu^{\text{QE}}$  of less than 10 GeV. The lower bound excludes a region where the expected flux of  $\nu_e$  and  $\bar{\nu}_e$  is small and the backgrounds are high. The upper bound eliminates events in the region of large flux uncertainty.

The reconstructed electron energy distribution of the 2105 selected  $\nu_e$  CCQE-like candidates is shown in Fig. 2 for both the data and the simulated event samples. The simulated sample is broken down by process according to the GENIE event generator and is 52% pure signal events. The primary source of background in the selected sample arises from  $\nu_e$ -induced non-CCQE-like events. The second largest background comes from incoherent neutral current (NC)  $\pi^0$  production. Coherent  $\pi^0$  production and neutrino-electron elastic scattering also contribute to the final sample.

The sizes of the backgrounds in Fig. 2 are constrained by two sideband samples. The first sideband consists of events at larger  $\Psi$ , which is enriched in inelastic backgrounds from  $\nu_e$

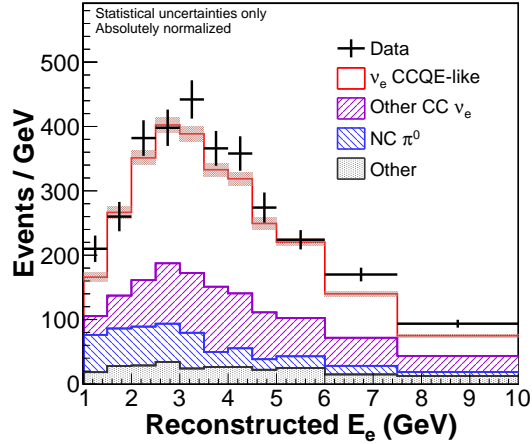


FIG. 2. The reconstructed electron energy distribution after all selection cuts and after constraining the backgrounds using sidebands in the data. The errors shown on the data are statistical only.

interactions and incoherent events containing  $\pi^0$ . The other sideband, dominated by  $\nu_e$  CC inelastic events, consists of events with Michel electron candidates. The normalizations of the  $\nu_e$  inelastic and incoherent  $\pi^0$  backgrounds are varied in order to find the best overall fit of simulation to the data in the reconstructed electron angle and reconstructed electron energy distributions in each sideband sample. Since, according to the simulation, the sideband in  $\Psi$  contains some signal events, the procedure is iterative. The background scale fit is done and the signal is extracted and used as a constraint for a new background scale fit. This is done until the background scale factors stabilize (two iterations). After this procedure, the fitted scale factor for the normalization for the  $\nu_e$  inelastic category is found to be  $0.89 \pm 0.08$ , while that for the incoherent  $\pi^0$  processes is  $1.06 \pm 0.12$ . The neutral-current coherent pion production is scaled down by a factor of two for pions with energies below 450 MeV in the simulation to bring the GENIE charged-current coherent charged pion production into agreement with a recent MINERvA measurement [33]. Subsequent to these constraints, the scaled backgrounds in the signal region are subtracted from the data.

An excess of photon or  $\pi^0$ -like events in the data relative to the simulation was observed in the distribution of energy deposited in the upstream part of the electron candidate cone, as characterized and described in detail in an accompanying paper[34]. Models of single photon or  $\pi^0$  production consistent with the observed excess were evaluated and found to have little effect on the background in the signal region of this analysis. Nevertheless, a  $\pi^0$

background fitted to the excess is added into the simulation and contributes (negligibly) to the background subtraction.

The flux-integrated differential cross sections in electron energy  $E_e$ , angle  $\theta_e$ , and four momentum transfer  $Q_{QE}^2$ , are calculated in bins  $i$  as a function of sample variable  $\xi$ , with  $\epsilon$  representing signal acceptance,  $\Phi$  the flux integrated over the energy range of the measurement (or over the bin  $i$ , in the case of the total cross-section),  $T_n$  the number of targets (nucleons) in the fiducial region,  $\Delta_i$  the width of bin  $i$ , and  $U_{ij}$  a matrix, derived from the simulation, correcting for detector smearing between bins  $i$  and  $j$  in the variable of interest:

$$\left(\frac{d\sigma}{d\xi}\right)_i = \frac{1}{\epsilon_i \Phi T_n (\Delta_i)} \times \sum_j U_{ij} \left( N_j^{\text{data}} - N_j^{\text{bknd pred}} \right). \quad (1)$$

$E_\nu^{\text{QE}}$  and  $Q_{QE}^2$  are calculated from the lepton kinematics alone using the approximation of a stationary target nucleon. Unfolding to correct for detector effects in the four variables is done using a Bayesian technique[35] with a single iteration.

The systematic errors considered arise from the primary neutrino interaction model, the flux model, and the detector response to particle activity. The errors on the flux are determined as discussed earlier. At the focusing peak, i.e., those neutrinos most relevant for this analysis, the  $\nu_e$  flux arises from muons from pion decays. The errors in the primary neutrino interaction model are evaluated via the reweighting of events by varying the underlying model tuning parameters according to their uncertainties. The parameters varied in this way include the shape and normalization for elastic and resonance productions, nuclear model parameters principally affecting the deep inelastic scattering, and parameters which control the strength and behavior of the final state interactions. Contributions to the detector response systematic error were determined by varying the energy scale for electromagnetic interactions, the parameter used in Birks' Law, the PMT cross-talk fraction, the Michel electron reconstruction energy scale, and the detector mass. The largest systematic errors contributing to the cross section results presented here are due to the detector response, interaction model and the flux model, with each contributing a fractional uncertainty of less than 10%. The overall systematic errors are typically in the 10-15% range, which is sufficiently small for the results presented here to be statistically limited.

The flux-integrated differential  $\nu_e$  CCQE-like cross sections versus electron energy and angle are given in Fig. 3, for both the data and the POT-normalized Monte Carlo samples. The analogous distribution in  $Q_{QE}^2$  is given on the left side of Fig. 4. The simulation appears

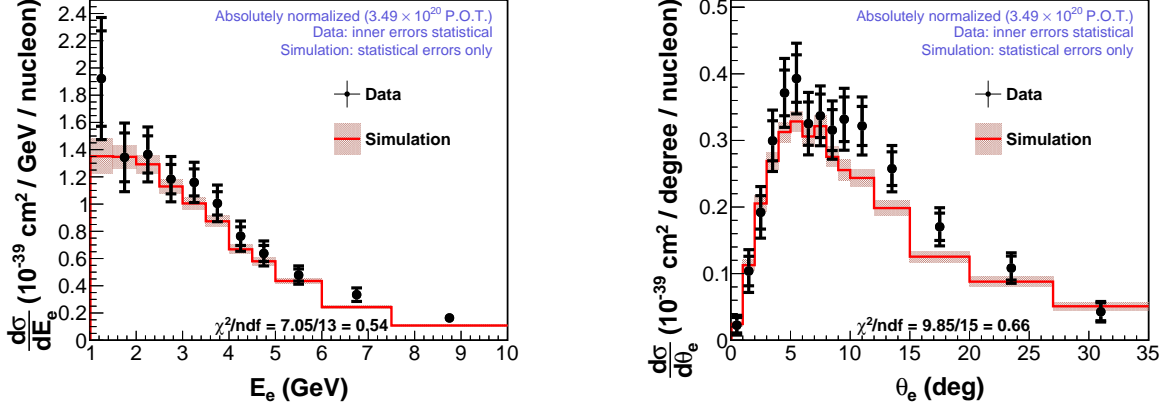


FIG. 3. Flux-integrated differential  $\nu_e$  CCQE-like cross section vs. electron energy (left) and electron angle (right). Inner errors are statistical; outer are statistical added in quadrature with systematic. The band represents the statistical error for the Monte Carlo curve.

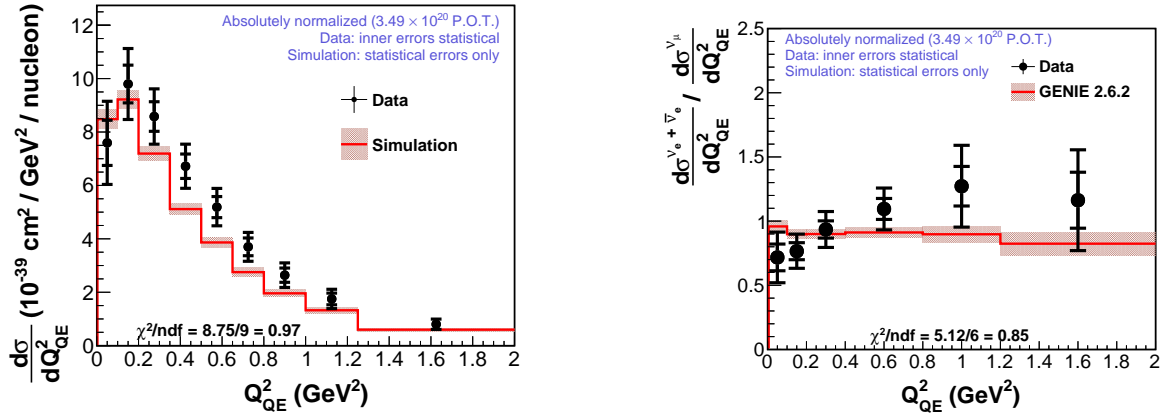


FIG. 4. The flux-integrated differential  $\nu_e$  CCQE-like cross section vs.  $Q_{QE}^2$  (left). Inner errors are statistical; outer are statistical added in quadrature with systematic. On the right is shown the ratio of the MINERvA  $\nu_e$  CCQE differential cross section as a function of  $Q_{QE}^2$  to the analogous result from MINERvA for  $\nu_\mu$ [32]. In both figures, the band represents the statistical error for the Monte Carlo curve.

to underestimate the width of the electron production angle and exhibit a harder spectrum in  $Q_{QE}^2$ . However, these differences are not significant when correlated errors, such as the electromagnetic energy scale, are taken into account.

In order to compare directly the measured differential cross section for  $\nu_e$  and  $\nu_\mu$  interactions on carbon as a function of  $Q_{QE}^2$ , an analysis similar to that described in this paper

was performed in terms of a CCQE signal (rather than CCQE-like), as specified by the GENIE event generator, which can be compared directly to previously published MINERvA results[32]. The selection cuts for the  $\nu_e$  events were adjusted slightly to ensure the energy range of included events agreed with that of the  $\nu_\mu$  analysis. The ratio of these two results and the corresponding ratio of the Monte Carlo predictions are given on the right in Fig. 4. The data for the differential cross section for  $\nu_e$  CCQE interactions agree within errors with that for  $\nu_\mu$  CCQE interactions.  $Q^2$ -dependent correlated errors, such as that in the electromagnetic energy scale, can cause trends in the data similar to the obvious upward slope in Fig. 4. Taking these correlated errors into account, the data is consistent with the GENIE prediction within  $1\sigma$ .

#### IV. CONCLUSIONS

This paper presents the first exclusive measurement of the flux-integrated differential cross section for  $\nu_e$  CCQE-like interactions, and thus provides the first data for directly testing and tuning models of a critical channel for accelerator-based oscillation experiments. The flux-integrated differential distributions of the cross section in  $E_e$ ,  $\theta_e$  and  $Q_{QE}^2$  agree with the expectation from lepton universality. A direct comparison, in the same detector, of the differential flux-integrated cross section of  $\nu_e$  CCQE interactions to that for  $\nu_\mu$  CCQE interactions as a function of  $Q_{QE}^2$  also shows good agreement. Collectively, these measurements constitute an important first test of the common assumption made by oscillation experiments that  $\nu_\mu$  cross section data can be applied to models of  $\nu_e$  CCQE interactions.

#### ACKNOWLEDGMENTS

This work was supported by the Fermi National Accelerator Laboratory under US Department of Energy contract No. DE-AC02-07CH11359 which included the MINERvA construction project. Construction support was also granted by the United States National Science Foundation under Award PHY-0619727 and by the University of Rochester. Support for participating scientists was provided by NSF and DOE (USA), by CAPES and CNPq (Brazil), by CoNaCyT (Mexico), by CONICYT (Chile), by CONCYTEC, DGI-PUCP and IDI/IGI-UNI (Peru), by Latin American Center for Physics (CLAF), and by RAS and the

Russian Ministry of Education and Science (Russia). We thank the MINOS Collaboration for use of its near detector data. We acknowledge the dedicated work of the Fermilab staff responsible for the operation and maintenance of the beamline and detector.

- 
- [1] D. S. Ayres *et al.* (NOvA Collaboration), *The NOvA Technical Design Report*, FERMILAB-DESIGN-2007-01 (2007).
  - [2] K. Abe *et al.* (T2K Collaboration), *Nucl. Instru. Methods* **659**, 106 (2011), arXiv:1106.1238.
  - [3] <http://www.dunescience.org/>.
  - [4] J. Blietschau *et al.* (Gargamelle Collaboration), *Nucl. Phys. B* **133** 205 (1978).
  - [5] K. Abe *et al.* (T2K Collaboration), *Phys. Rev. Lett.* **113** 241803 (2014), arXiv:1407.7389.
  - [6] M. Day and K. S. McFarland, *Phys. Rev. D* **86**, 053003 (2012), arXiv:1206.6745.
  - [7] O. Lalakulich, U. Mosel, and K. Gallmeister, *Phys. Rev. C* **86**, 054606 (2012), arXiv:1208.3678.
  - [8] M. Martini and M. Ericson, *Phys. Rev. C* **87**, 065501 (2013), arXiv:1303.7199.
  - [9] J. Nieves, M. Valverde, and M. J. Vicente Vacas, *Phys. Rev. C* **73**, 025504 (2005), arXiv:0511204.
  - [10] K. Anderson, B. Bernstein, D. Boehnlein, K.R. Bourkland, S. Childress *et al.*, The NuMI Facility Technical Design Report No. FERMILAB-DESIGN-1998-01, 1998; P. Adamson *et al.*, arXiv:1507.06690 (2015).
  - [11] S. Agostinelli *et al.*, *Nucl. Instru. Methods A* **506**, 250 (2003).
  - [12] J. Allison *et al.*, *IEEE Trans. Nucl. Sci.* **53**, 270 (2006).
  - [13] C. Alt *et al.* (NA49 Collaboration), *Eur. Phys. J. C* **49**, 897 (2007).
  - [14] D. S. Barton *et al.*, *Phys. Rev. D* **27**, 2580 (1983).
  - [15] B. Baatar *et al.*, *Eur. Phys. J. C* **73**, 2364 (2013).
  - [16] S.P. Denisov *et al.*, *Nucl. Phys. B* **61**, 62 (1973).
  - [17] A.S. Carroll *et al.*, *Phys. Lett. B* **80**, 319 (1979).
  - [18] N. Abgrall *et al.*, *Phys. Rev. C* **84**, 034604 (2011).
  - [19] G. Tinti, *Sterile neutrino oscillations in MINOS and hadron production in pC collisions*, Ph.D. thesis, Oxford University (2010).
  - [20] A. Lebedev, *Ratio of pion to kaon production in proton carbon interactions*, Ph.D. thesis, Harvard University (2007).

- [21] J. V. Allaby *et al.*, Phys. Lett. **B30**, 500 (1969).
- [22] FTFP shower model in GEANT4 version 9.2 patch 03.
- [23] Z. Pavlovic, *Observation of Disappearance of Muon Neutrinos in the NuMI Beam*, Ph.D. thesis, University of Texas (2008).
- [24] J. Park, *Neutrino-electron scattering in MINERvA for constraining the NuMI neutrino flux*, Ph.D. thesis, University of Rochester (2013).
- [25] D.G. Michael *et al.* (MINOS Collaboration), Nucl. Instru. Methods **A596**, 190 (2008).
- [26] L. Aliaga *et al.* (MINERvA Collaboration), Nucl. Instru. Methods **A743** 130 (2013), arXiv:1305.5199.
- [27] L. Aliaga *et al.* (MINERvA Collaboration), Nucl. Instru. Methods **A789** 28 (2015), arXiv:1501.06431.
- [28] G. N. Perdue *et al.*, Nucl. Instru. Methods **A694** 179 (2012), arXiv:1209.1120.
- [29] C. Andreopoulos, A. Bell, D. Bhattacharya, F. Cavanna, J. Dobson, S. Dytman, H. Gallagher, P. Guzowski, R. Hatcher, P. Kehayias, A. Meregaglia, D. Naples, G. Pearce, A. Rubbia, M. Whalley, And T. Yang, Nucl Instrum. Methods **A614**, 87 (2010), program version 2.6.2 used here.
- [30] C.H. Llewellyn Smith, Phys. Rep. **3**, 261 (1972).
- [31] T. Hastie, R. Tibshirani, and J. Friedman, **The elements of statistical learning**, Springer, New York, second edition, 2009.
- [32] G. A. Fiorentini *et al.* (MINERvA Collaboration), Phys. Rev. Lett. **111**, 022502 (2013), arXiv:1305.2243.
- [33] A. Higuera *et al.* (MINERvA Collaboration), Phys. Rev. Lett. **113** 261802 (2014), arXiv:1409.3835.
- [34] J. Wolcott *et al.* (MINERvA Collaboration), to be published.
- [35] G. D'Agostini, Nucl. Instru. Meth. **A362**, 487 (1995).